



PCCP

How polymer additives reduce the pour point of hydrocarbon solvents containing wax crystals

Journal:	<i>Physical Chemistry Chemical Physics</i>
Manuscript ID:	CP-ART-09-2014-004329.R2
Article Type:	Paper
Date Submitted by the Author:	18-Dec-2014
Complete List of Authors:	Binks, Bernie; University of Hull, Department of Chemistry; University of Hull, Department of Chemistry Fletcher, P; University of Hull, Department of Chemistry Roberts, Noel; University of Hull, Department of Chemistry Dunkerley, John; Lubrizol Ltd., Greenfield, Hannah; Lubrizol Ltd., Mastrangelo, Antonio; Lubrizol Ltd., Trickett, Kieran; Lubrizol Ltd.,

SCHOLARONE™
Manuscripts

How polymer additives reduce the pour point of hydrocarbon solvents containing wax crystals

Bernard P. Binks, Paul D.I. Fletcher* and Noel A. Roberts
*Surfactant & Colloid Group, Department of Chemistry,
University of Hull, Hull. HU6 7RX. U.K.*

John Dunkerley, Hannah Greenfield, Antonio Mastrangelo and Kieran Trickett
Lubrizol Limited, The Knowle, Nether Lane, Hazelwood, Derby, Derbyshire DE56 4AN

*Author for correspondence: Prof. P.D.I. Fletcher
E mail: P.D.Fletcher@hull.ac.uk

Abstract

We have investigated how four different pour point depressant (PPD) polymers affect the pour point transition in mixtures of a single pure wax in a solvent. We used either *n*-eicosane (C20), $\text{CH}_3(\text{CH}_2)_{18}\text{CH}_3$, *n*-tetracosane (C24), $\text{CH}_3(\text{CH}_2)_{22}\text{CH}_3$ or *n*-hexatriacontane (C36), $\text{CH}_3(\text{CH}_2)_{34}\text{CH}_3$ as the wax component with either *n*-heptane or toluene as the solvent component. For all wax/solvent combinations, the measured variation of wax solubility with temperature is well predicted by ideal solution theory. The variation of pour point temperature as a function of the overall wax concentration is quantitatively modelled using the idea that, for each overall wax concentration, the pour point occurs at a temperature at which a critical volume fraction ϕ^* of wax crystals has precipitated. Close to the pour point temperature, extraction and examination of the wax crystals show they consist of polydisperse, irregularly-shaped platelets with axial ratios (h/d , where h is the plate thickness and d is the plate long dimension) in the range 0.005-0.05. It is found that the measured ϕ^* values corresponding to the pour point transitions are weakly correlated with the wax crystal axial ratios (h/d) for all wax/solvent/PPD polymer combinations. These results indicate that the pour point transition occurs at a volume fraction larger than the value at which the volumes of rotation of the platelet crystals overlap, i.e., $2.5(h/d) < \phi^* < 11(h/d)$. PPD polymers work, in part, by increasing the wax crystal axial ratio (h/d), thereby increasing ϕ^* and reducing the pour point temperature. Since the PPD's ability to modify the wax crystal shape relies on its adsorption to the crystal-solution surface, it is anticipated and observed experimentally that optimum PPD efficacy is correlated with the difference between the wax and the polymer solubility boundary temperatures. This finding and the mechanistic insight gained here provide the basis for a simple and rapid screening test to identify candidate species likely to be effective PPDs for particular wax systems.

1. Introduction

When a solution of a long chain hydrocarbon wax in a hydrocarbon solvent is cooled, wax crystals are formed at temperatures below the solubility boundary temperature of the solution. Upon further cooling, sufficient wax crystals are produced to form a crystal network throughout the two-phase dispersion of wax crystals plus saturated wax solution. The crystal network causes gel formation and the mixture exhibits a finite yield stress and ceases to pour (flow) as a result of gravity¹⁻³. The temperature at which this occurs is called the pour point temperature and it depends primarily on the solvent, the nature of the wax and its concentration. Failure to flow caused by wax crystallisation is a major problem for pipeline transport of crude oils and the use of hydrocarbon fuels in cold climates. The importance of enhancing our understanding of crystal network formation is not limited to petrochemical applications. Commercial products such as shoe polish consist of a semi-solid wax crystal network within a matrix of saturated solution. In addition, the processing of liquid triacylglyceride (TAG) oil mixtures into semi-solid fat products such as butter and margarine involves the precipitation of the high melting point TAG components. The system forms a gelled fat crystal network which, in turn, determines many key properties of the final semi-solid fat product⁴.

For hydrocarbon wax/solvent mixtures, polymer additives are used to reduce the pour point temperature – so called “pour point depressants” (PPDs). There is extensive literature on the efficacy of different PPD chemical structures in reducing the pour point temperatures of different wax/solvent mixtures⁵⁻³³. It is believed that the pour point reduction observed for a particular PPD/wax/solvent system is related to the interactions of the PPD with particular faces of the growing wax crystals. Computer simulation has been used to probe these interactions in certain systems³⁴⁻³⁶. However, despite these extensive previous studies, many fundamental questions about both the basic mechanism of the pour point phenomenon and how PPDs affect the pour point are currently not fully resolved. These questions include:

1. Can the wax solubility as a function of temperature be quantitatively predicted?
2. What is the volume fraction of the precipitated wax crystals present at the pour point temperature?
3. How does the volume fraction of the precipitated wax crystals present at the pour point temperature depend on the crystal properties? Can this information be used to predict the pour point temperatures for a particular wax/solvent system?
4. How does the addition of a polymer PPD affect points 1-3 above? Does this information provide guiding principles to enable the rapid screening of PPDs for their likely efficacy?

The aims of this work are to address questions 1-4 above using model systems consisting of a single wax component with a single solvent component with and without a polymeric PPD. The model systems consist of either *n*-eicosane, $\text{CH}_3(\text{CH}_2)_{18}\text{CH}_3$, *n*-tetracosane, $\text{CH}_3(\text{CH}_2)_{22}\text{CH}_3$ or *n*-hexatriacontane, $\text{CH}_3(\text{CH}_2)_{34}\text{CH}_3$ as the wax component with either *n*-heptane or toluene as the solvent component. Four different PPD polymers were used, as shown in ESI Table 1. The polymer abbreviated names have the format “x-y-z” where x indicates the molecular mass (HMn = high number average molecular mass and LMn = low), y indicates the monomers used (M = maleic anhydride, S = styrene and A = methyl methacrylate) and z indicates the hydrocarbon side chain length. Thus, HMn-MS-C18-22 and LMn-MS-C18-22 are both maleic anhydride-styrene copolymers (1:1 monomer mole ratio) with C18-22 side chains; they differ only in their average molecular mass. LMn-MSA-C18-22 and LMn-MSA-C12 are both maleic anhydride-styrene-methyl methacrylate copolymers (1:1:0.05 monomer mole ratio) of similar average molecular mass; they differ only in the lengths of the hydrocarbon side chains.

2. Experimental

2.1 Materials.

n-Eicosane (abbreviated to C20, Sigma-Aldrich, 99%), *n*-tetracosane (abbreviated to C24, Sigma-Aldrich, 99%), *n*-hexatriacontane (abbreviated to C36, Sigma-Aldrich, 98%), *n*-heptane (Fischer Scientific, 99%) and toluene (Fischer Scientific, 99.99%) were used as received. The four polymeric PPDs and their characterisation data (see electronic supplementary material ESI Table 1) were supplied by Lubrizol Ltd., Hazelwood, UK. Polymer LMn-MSA-C12 was supplied as the pure liquid polymer. The other three polymers were supplied as 90 wt% polymer dispersions in toluene; the toluene solvent was removed prior to use by drying to constant mass under vacuum at 50 °C.

2.2 Methods.

Solubility measurements of the wax and PPD polymers in the solvents were made by weighing the required masses into 4 mL clear, squat-form vials which were screw top sealed to prevent evaporation loss of the solvent. These were then placed in a Grant LTD 6/20 water bath with Grant LTD6G heating unit and preheated to 75°C for five minutes to ensure the sample was fully dissolved and homogeneous. The water bath temperature was then decreased at 0.3°C/min to obtain a rough value of the temperature at which precipitated wax or PPD is first observed using a 5x magnification hand lens (T_{cool}). For each visual observation, samples were removed from the water bath for no more than a few seconds and gently shaken before being replaced. Following the rough measurement of T_{cool} , more accurate measurements of both T_{cool} and T_{heat} (the temperature at which the last trace of precipitate was observed to disappear on heating the sample) were made at slower cooling/heating rates of 0.1°C/min. Temperature measurements were made using a $\pm 0.1^\circ\text{C}$ thermocouple (Omega MH806WE) calibrated with a $\pm 0.1^\circ\text{C}$ ASTM calibrated total immersion thermometer.

Pour point temperatures were measured using a slightly modified version of the ASTM D97 procedure³⁷. The pour point temperature was taken to be the highest temperature at which no flow of the sample was observed when the vessel was tilted from vertical to horizontal. Experimentally, this temperature was found to be equal (within the experimental uncertainty of $\pm 0.2^\circ\text{C}$) to the lowest temperature at which movement of the sample was observed on tilting. A first rough value was obtained by cooling the sample at 0.3°C/min. Final values of the pour point temperatures from both cooling and heating used temperature change rates of 0.1°C/min. For selected systems, it was found that heating or cooling produced no significant changes in the pour point temperatures and the majority of measurements were made using cooling only. In principle, the frequency of tilting the sample may disturb the network of precipitated wax crystals and hence affect the pour point. In practice, we found that using variable times (from 20 s to several minutes) between tilting of the sample in the determination of the pour point did not significantly affect the final pour point temperature within the uncertainty of $\pm 0.2^\circ\text{C}$.

Wax crystals were extracted from two-phase mixtures at temperatures below the solubility boundary and imaged using scanning electron microscopy (SEM) as follows. A sample of the required composition was first fully dissolved by holding it at a temperature of few °C above T_{heat} for ten minutes. It was then cooled to a temperature within 2 °C or less (most samples were within 0.5 °C) of its pour point temperature and held at this temperature for 2 minutes. The solutions were then rapidly (less than 10 seconds) vacuum filtered using paper filter discs (Sartorius stedim, grade 292, particle retention 5-8 μm) at room temperature of 18-22 °C. The wax crystals had the appearance of a slightly damp powder at this point; they were held in a continuously evacuated vacuum desiccator at 18-22 °C for 60 hours to remove traces of residual solvent. A random selection of wax crystals was carefully sprinkled from the filter paper onto a carbon impregnated 'sticky disc' (12 mm diameter carbon-based, electrically conducting disc coated on both faces with polycarbonate

adhesive supplied by Agar Scientific) attached to a 15 mm diameter threaded Hitachi SEM mount. This sprinkling procedure was used to minimise possible breaking of the crystals. The sample was imaged at various magnifications using an Hitachi TM-1000 SEM operating at 15 kV with a vacuum of 50 Pa. These conditions were selected to minimise electron beam “melting” and surface charging artefacts of the wax crystals. Preliminary experiments using a Zeiss EVO 60 SEM operating at 20 kV produced significant melting of the C20 and C24 waxes.

3. Results and Discussion

3.1 Wax solubility as a function of temperature

As shown in the electronic supplementary material (ESI Figure 1) we observe a hysteresis of a few °C in measurements of the solubility boundary temperatures by cooling and heating, T_{cool} and T_{heat} . Since the solubility boundary is an equilibrium quantity, this hysteresis must result from the kinetics of either the crystal formation or dissolution being slow relative to the temperature change rate used here (0.1 °C/min). Crystal formation by cooling occurs by nucleation and growth which generally requires an energy barrier to be overcome and hence can be slow. Crystal dissolution by heating is expected to require little or no energy barrier and is likely to be fast. Hence, T_{heat} is expected to correspond to the true, equilibrium temperature of the solubility boundary. This expectation is confirmed by the experimental results shown in ESI Figure 1 and we therefore take T_{heat} values to be equal to the *equilibrium* solubility boundary temperatures.

Figure 1 shows the variation of wax solubility with temperature for the three pure waxes in both heptane and toluene. In order to quantitatively predict the solubility behaviour, we assume that the wax/solvent mixtures form ideal solutions and that the wax crystals contain no co-crystallised solvent. In the case of a pure wax which, in the absence of solvent, shows only a single phase transition from crystalline solid to a liquid at a temperature T_{liq} with molar enthalpy change ΔH_{liq} , the variation of solubility with temperature is given by³⁸⁻³⁹:

$$\ln X = \frac{-\Delta H_{\text{liq}}}{R} \left(\frac{1}{T} - \frac{1}{T_{\text{liq}}} \right) \quad (1)$$

where X is the mole fraction of solute in the saturated solution at absolute temperature T and R is the gas constant. As seen in Table 1, the waxes C24 and C36 show more complex phase behaviour. They form a crystalline solid at temperatures less than T_{rot} at which a rotator phase forms with molar enthalpy change ΔH_{rot} . The rotator phase transforms to the liquid at temperature T_{liq} with molar enthalpy change ΔH_{liq} . To take account of the rotator phase formation, the solubility equation must be modified as shown below.

$$\ln X = \frac{-\Delta H_{\text{liq}}}{R} \left(\frac{1}{T} - \frac{1}{T_{\text{liq}}} \right) \quad \text{for } T_{\text{rot}} < T < T_{\text{liq}} \quad (2)$$

$$\text{and } \ln X - \ln X_{\text{rot}} = \frac{-(\Delta H_{\text{liq}} + \Delta H_{\text{rot}})}{R} \left(\frac{1}{T} - \frac{1}{T_{\text{rot}}} \right) \quad \text{for } T < T_{\text{rot}} \quad (3)$$

where X_{rot} is the mole fraction of solute in the saturated solution at absolute transition temperature T_{rot} (determined using equation 2).

Using literature values of the transition temperatures and enthalpies⁴⁰⁻⁴⁷ given in Table 1, equations 1-3 were used to calculate the variation of wax solubility with temperature as shown by the curved dashed lines in Figure 1. The agreement with the measured data points is within the estimated

uncertainties (± 0.5 °C or so) in all the wax/solvent combinations except for the C20/toluene system where small but significant deviations are observed. Overall, the conclusion is that the equilibrium solubility behaviour of these wax/solvent systems is adequately predicted by ideal solution theory requiring no adjustable parameters as input. This conclusion is in reasonable agreement with previous studies of single wax/alkane solvent systems; however, it is noted that prediction of the solubility behaviour of wax mixtures is considerably more complex⁴⁸⁻⁶⁶.

3.2 Pour point temperature versus wax concentration with and without polymer PPD additives

Figure 2 shows two examples of measured pour point temperatures as a function of the wax concentration for systems without PPD additives. It can be seen that the measured pour point curves are similar to the corresponding solubility boundaries but simply shifted on the wax concentration scale. In order to model the pour point temperature curves, we postulate that the pour point temperature corresponds to the temperature at which a critical volume fraction ϕ^* of wax crystals has precipitated, just sufficient to create a gelled crystal network causing the pour point transition. The value of ϕ^* is assumed to be independent of the overall wax concentration for a particular wax/solvent system but specific to each wax/solvent system. Using equations 1-3, we calculate the temperature at which a set volume fraction of crystals is precipitated as a function of the overall wax concentration. For each wax/solvent system, the critical volume fraction ϕ^* of crystals is adjusted to obtain the best fit with the experimental pour point curve as shown in Figure 2. The pour point curves calculated in this way show good agreement with the experimental data; thereby justifying the assumption that ϕ^* is independent of the wax concentration. As seen in Table 2, the values of ϕ^* for the different wax/solvent systems in the absence of PPD polymer vary from 1.5 to 7.4 vol%. Some possible reasons for this variation of ϕ^* for the different systems are discussed in section 3.3.

The addition of 1 wt% PPD polymer has different effects on the pour point curve which appear to depend primarily on the temperature of the polymer solubility boundary relative to the wax solubility boundary temperature. Illustrative plots comparing pour point curves with and without PPD, wax solubility curves and the PPD solubility boundary are shown in Figure 3. In the upper plot (C20 wax, heptane solvent, 1 wt% LMn-MSA-C18-22), the polymer solubility boundary occurs at approx. 27 °C (the polymer is soluble above this temperature and precipitates below it). This temperature is much higher than the wax solubility boundary temperatures of -10 to 10 °C at 0-20 wt% wax. Hence, over the temperature range at which the wax precipitates to cause the pour point transition, the concentration of dissolved polymer is expected to be low and hence little or no effect of polymer addition on the pour is expected. In agreement with this prediction, the pour point curves with and without polymer are not significantly different. It appears that the presence of the *precipitated* polymer does not significantly affect the pour point temperature.

In the middle plot (C36 wax, heptane solvent, 1 wt% LMn-MS-C18-22), the polymer solubility boundary in the absence of wax occurs at 26 °C. This is below, but within, the range of the wax solubility boundary temperatures of 20 to 50 °C at 0-20 wt% wax. In this case, the polymer is fully dissolved over the relevant temperature range but rather close to precipitating, indicating that the polymer affinity for the solvent is low. A low affinity between polymer and solvent is expected to maximise the tendency of the polymer to leave the solution by adsorption to the wax crystals. Strong adsorption of the polymer to the wax crystals is then likely to produce a significant effect on the pour point curve. It can be seen that there is indeed a large reduction in pour point temperatures for this system by up to 17 °C. As seen in Table 2, this large pour point depression effect can be quantified in terms of ϕ^* . In the absence of polymer, ϕ^* is 2.9 vol% whereas the addition of 1 wt% of the polymer increases ϕ^* to 13.6 vol%. For wax concentrations less than about 15 vol% when the fitted pour point curve lies below the polymer solubility temperature, the measured pour point

temperatures no longer follow the fitted pour curve; instead they are approximately equal to the polymer solubility temperature. For this reason, the low wax concentration data points (below approx. 15 wt%) were excluded when fitting the pour point curve to estimate ϕ^* . Overall, the extent of reduction of the pour point temperature appears to be limited by the onset of the polymer precipitation.

In the lower plot (C20 wax, heptane solvent, 1 wt% LMn-MSA-C12), the polymer solubility boundary occurs below $-10\text{ }^\circ\text{C}$ (and was not measured), much lower than the range of the wax solubility boundary temperatures of -10 to $10\text{ }^\circ\text{C}$ at 0-20 wt% wax. In this case, the polymer is fully dissolved over the relevant temperature range and also far from precipitating, indicating that the polymer affinity for the solvent is high. A high affinity between polymer and solvent is expected to maximise the tendency of the polymer to remain in solution. Hence, adsorption to the wax crystals and the corresponding effect on the pour point curve, are likely to be small. It can be seen that there is indeed only a small effect on the pour point temperatures for this system. As seen in Table 2, ϕ^* is 5.5 vol% in the absence of polymer and 7.1 vol% in the presence of 1 wt% of the polymer.

Although we mainly focus here on the effects of adding 1 wt% of the PPD polymers, measurements have been made for different PPD polymer concentrations, as shown in the electronic supplementary material. ESI Figure 2 shows the variation of polymer solubility temperature with polymer concentration in both heptane and toluene solvents. For the case of heptane, the three polymers measured all show solubility temperatures that are virtually independent of the polymer concentration from 0.005 to 5 wt%. Hence, these polymer/solvent systems switch from being virtually either fully soluble or fully precipitated as the solubility temperature boundary is crossed. For toluene as solvent, the change in polymer solubility with temperature is much more gradual.

ESI Figure 3 shows some examples of the effects of PPD concentration on the variation of pour point temperature with wax concentration. For the C24/toluene/LMn-MSA-C12 system (for which the addition of 1 wt% gives no change in the pour point temperatures), it can be seen that the pour point curve is unaffected by the addition of 0.5 – 2 wt% LMn-MSA-C12. In contrast, the pour point plots for the C24/toluene/LMn-MSA-C18-22 system (for which 1 wt% PPD addition causes a pour point temperature reduction corresponding to an increase in ϕ^* from 4.0 to 13.2 vol%) shift progressively to lower temperatures as the LMn-MSA-C18-22 concentration is increased from 0.5 to 2 wt%. This shift is not observed for wax concentrations less than about 15 vol% where the pour point reduction is limited by precipitation of the polymer. Overall, these and similar results for other wax/solvent/PPD systems (not shown) show that changing the PPD polymer concentration has no effect for ineffective PPDs whereas the effect increases when the PPD concentration is increased from 0.5 to 2 wt% for those PPDs which are effective.

3.3 *How is ϕ^* related to the properties of the precipitated wax crystals?*

From the results discussed in section 3.2, it can be seen that the variation of pour point temperature with the overall wax concentration is reasonably accurately described by a model based on the idea that the pour point transition occurs at a critical volume fraction of crystals (ϕ^*) which is independent of the overall wax concentration. The value of ϕ^* is specific to each particular wax/solvent system and can be changed by the addition of PPD polymers. As seen in Table 2, we observe that ϕ^* is in the range of 1.5 to 14.8 vol% for the systems investigated here.

As discussed in ref. 67, gel formation by particle dispersions occurs by inter-particle attraction leading to particle aggregation to form a sample-spanning network having a finite yield stress. For the case of spherical particles with short-range attraction, gelation is initiated by spinodal

decomposition at the equilibrium gas-liquid phase boundary of the dispersion⁶⁷. Gel formation in waxy crude oils has been shown to exhibit similar rheological behaviour to gels formed from fumed silica particles dispersed in paraffin oil². For the wax/solvent systems investigated here, the gelling particles consist of wax crystals which are triclinic for C20 and C24 and monoclinic for C36. Theoretical and experimental crystal shapes and corresponding relative face growth rates of alkane waxes have been reported⁶⁸⁻⁷⁵. Crystals of the triclinic even n-alkanes consist of flat plates with large, slow growing {001} flat faces exposing terminal methyl groups and small, fast growing edge faces which expose mainly methylene groups. Theoretical estimates of the crystal axial ratios (small/large dimension) are of the order 0.01, similar to what is observed here. The difference in surface energy between the low energy methyl-exposing {001} surface and the higher energy methylene-exposing edge faces is expected to be approximately 8 mJ m^{-2} ⁷⁶. This surface energy difference between the crystal flat and edge faces is expected to be important in controlling the relative strengths of flat-flat, flat-edge and edge-edge adhesion contacts in the aggregation process leading to the gelled crystal network.

There has been extensive study of the phase behaviour of dispersions of hard discs of thickness h and diameter d . For hard discs of axial ratio h/d , the volume fraction at which their spheres of revolution overlap $\phi_{\text{overlap}} \approx 1.1(h/d)$. Both theoretically and experimentally, hard disc dispersions show a transition from an isotropic to nematic liquid crystalline phase at a volume fraction $\phi_{\text{I-N}} \approx 3(h/d)$ ⁷⁷⁻⁸⁹. Wu et al.⁸⁸ have shown that addition of a spherical attractive square well potential at the centre of mass of the discs facilitates the formation of orientationally ordered phases.

The SEM micrographs of Figure 4 show that the wax crystals extracted at temperature close to the pour point temperatures consist of irregularly shaped, polydisperse, thin platelets. The isotropic dispersion-gel transition (as opposed to an isotropic-nematic phase transition) presumably occurs because the crystals are (i) irregularly shaped, (ii) polydisperse and (iii) likely to possess attractive dispersion inter-particle attractions which are different for the crystal flat faces and edges. Despite these differences between the wax crystals and hard discs, it seems reasonable to speculate that the pour point critical volume fraction ϕ^* might be related to ϕ_{overlap} and hence (h/d) . In addition, if gel formation is initiated by a phase transition as discussed in ref. 67, ϕ^* might be better correlated with $\phi_{\text{I-N}}$ which again depends on (h/d) . We hypothesise here that $\phi^* = x(h/d)$ where x is an (unknown) constant but note that we cannot exclude the possibility that ϕ^* might also depend on (as yet unidentified) factors other than the crystal axial ratio (h/d) such as crystal-crystal adhesion forces.

In order to test the hypothesis that $\phi^* = xh/d$, it is necessary to determine average values of the wax crystal dimensions h and d . This is a very challenging experimental task since h is of the order 0.1-1 μm whereas d is of the order 10-100 μm . The wax crystal plate thickness is typically too small to be resolved by visible light microscopy and hence methods such as confocal fluorescence microscopy cannot be used to determine the crystal morphology *in situ* within the samples. Because the higher resolution of scanning electron microscopy (SEM) is required, the wax crystals must be extracted from the samples as described in the experimental section. This procedure has the disadvantage that some crystal breaking may occur during the extraction. In addition, the determination of average values of h and d from the SEM micrographs has a low precision caused by the intrinsic difficulties of resolving h and d values for individual crystals within the SEM images (see ESI Figure 4). Despite these challenges causing large uncertainties in the values of h/d , we report results in Table 2 for the different wax/solvent systems with and without PPD polymer in order to test (for the first time) for a possible correlation between ϕ^* and (h/d) .

Figure 5 shows examples of cumulative distributions of h and d derived from SEM images similar to the examples in Figure 4. ESI Figure 4 shows SEM images labelled with the arrowed dimensions of the individual crystals which were used to construct the corresponding distribution plot. For each distribution plot a total of at least 40-60 values of d and 20-30 values of h were recorded from six separate images covering different sample areas at different magnifications. For each system, the average value of h/d was calculated using the h and d values corresponding to the 50% cumulative frequency point on the distribution plot and values are summarised in Table 2. It was checked (ESI Figure 5) that the cumulative distributions of h and d were not significantly affected (within the estimated uncertainties in h (approx. $\pm 40\%$) and d (approx. $\pm 30\%$); see ESI Table 2 for the results of repeated experiments) by changing the wax concentration from 20 to 40 wt%. As seen in ESI Figure 5, larger variations in h and d were observed by changing how the wax crystal sampling temperature was reached (slow or fast cooling from above or heating from below the final temperature). These latter variations can be seen to be similar in magnitude to the estimated uncertainties and so may have limited significance.

Figure 6 shows a plot of ϕ^* versus h/d for all the systems where it can be seen that there is only a weak correlation between ϕ^* and (h/d) ; the Pearson product-moment correlation coefficient is 0.645. It is observed here that the entire data set falls within the dashed lines corresponding to $2.5(h/d) < \phi^* < 11(h/d)$. We conclude that, although there is a weak correlation between ϕ^* and crystal axial ratio, it appears that ϕ^* is not *solely* determined by the value of (h/d) , either in the presence or absence of PPD polymer. Additional factors such as wax crystal-wax crystal adhesion must also affect ϕ^* . Examination of Table 2 indicates that the addition of an effective PPD polymer (indicated by an increase in ϕ^* relative to the corresponding value in the absence of PPD) again weakly correlates with an increase in (h/d) for the wax crystals in the presence of the PPD polymer relative to that in the absence. Hence, at least in part, effective PPD polymers decrease the pour point temperature by increasing the wax crystal axial ratio (h/d) but are also likely to affect other contributory factors such as crystal-crystal adhesion.

3.4 Under what conditions are PPD polymers effective?

The results of section 3.3 indicate that effective PPD polymers decrease the pour point temperature partly by increasing the axial ratio (h/d) of the precipitated wax crystals. It is thought that modification of crystal shapes by an additive such as a PPD polymer occurs by differential adsorption of the additive to the different faces of the growing crystal which, in turn, alters the growth rates of the different faces thereby changing the final axial ratio. Hence, for a PPD to be effective, (i) it must adsorb from solution to the crystal-solution interface and (ii) the adsorption to the plate-like crystal edge and flat faces must be different and/or modify the growth rates differently. In order to increase (h/d) , the edge face growth rate of the wax platelet crystals must be slowed more than the growth rate of the plate faces. In general, the tendency of a polymer to adsorb from solution to a crystal-solution interface depends on the relative affinities of the polymer for the solvent and for the crystal surface. For the PPD polymers and solvents used here, we observe that the polymers are soluble at high temperatures and precipitate as the temperature is reduced. The temperature at which the polymer becomes insoluble provides a crude relative measure of the polymer-solvent affinity. If the solubility temperature is very low, the polymer has high affinity for the solvent and low adsorption to the crystals is expected. If the solubility temperature is very high (and well above the experimental temperature), the bulk of the polymer precipitates and the concentration of dissolved polymer is too low for strong adsorption. Overall, the highest tendency to adsorb is expected to occur at temperatures above but close to the solubility temperature. Based on these considerations, it is expected that PPD polymers with polymer solubility temperatures slightly below the wax solubility temperatures of the wax/solvent systems have the potential to be effective in reducing the

pour point temperature. However, it must be noted that, although systems fulfilling this condition of the relative temperatures are likely to show optimal adsorption, they may not exhibit the strong *differential* adsorption to the crystal edges and faces necessary to increase (h/d) and reduce the pour point temperature. Hence, if these ideas are correct, we expect effective PPD polymer/wax/solvent systems to be within this “window” of relative temperatures but also that not all systems within the “window” will necessarily be effective.

In order to test this idea, we have plotted the change in pour point depression effectiveness (expressed as the change in critical volume fraction of precipitated wax crystals ($\phi^*_{1\text{wt}\% \text{PPD}} - \phi^*_{\text{noPPD}}$) versus the difference between wax and polymer PPD solubility temperatures ($T_{\text{heat}1\text{wt}\% \text{PPD}} - T_{\text{heat}20\text{wt}\% \text{wax}}$) for all the different systems. As seen in Figure 7, the plot shows a maximum, consistent with the ideas of relative solvent affinity and adsorption tendency discussed above. Overall, the pour point reduction for systems containing 20 wt% wax is most effective when the solubility temperature of the PPD polymer in the solvent is about 15 °C below that of the target wax/solvent system. Although the optimum temperature difference is -15 °C, the “window” of temperature difference in which effective PPD action is observed extends at least 20 °C either side of the optimum value. In Figure 7, the PPD effectiveness expressed as ($\phi^*_{1\text{wt}\% \text{PPD}} - \phi^*_{\text{noPPD}}$) is plotted versus ($T_{\text{heat}1\text{wt}\% \text{PPD}} - T_{\text{heat}20\text{wt}\% \text{wax}}$), corresponding to systems containing 20 wt% wax. ESI Figure 6 shows similar plots for systems containing either 50 wt% wax or 100 wt% wax (for which $T_{\text{heat}100\text{wt}\% \text{wax}}$ is equal to the melting temperature of the pure wax). It can be seen that maxima similar to that in Figure 7 occur in all the plots but that the optimum temperature difference shifts from -15°C for 20 wt% wax to -25°C for 50 wt% wax to -41°C for 100 wt% wax.

These results indicate that measurement of the polymer/solvent solubility temperature could provide an easy screening test for the rapid identification of candidate PPD species likely to be effective pour point depressants for wax/solvent systems which precipitate at a particular temperature. Further work is underway to see whether this potentially very useful result holds true for a wider range of PPD chemical types than those used here.

Conclusions

The aims of this work were to answer the four questions posed in the introduction and thereby elucidate how PPD additives reduce pour point temperatures. The key conclusions are as follows:

1. The solubility as a function of temperature for linear chain waxes in heptane and toluene can be accurately predicted using ideal solution theory and the phase transition temperatures and enthalpies for the pure waxes.
2. Plots of pour point temperature versus the overall wax concentration are reasonably accurately modelled by assuming that the pour point occurs at a temperature at which a wax concentration-independent, critical volume fraction ϕ^* of wax has precipitated. Values of ϕ^* are observed to be in the range of 0.015-0.15 for the different systems.
3. Precipitated wax crystals have been extracted and imaged using SEM. They consist of thin, polydisperse and irregularly-shaped platelets with (approximate) axial ratios (h/d) in the range 0.005-0.05.
4. The range of measured values of ϕ^* correlate weakly with measured (but rather low accuracy) values of the axial ratios (h/d) of precipitated wax crystals. Values of ϕ^* are found to be between 2.5(h/d) and 11(h/d), higher than the estimated overlap volume fraction. The

weakness of the correlation between ϕ^* and (h/d) indicate that ϕ^* is not solely determined by the crystal axial ratio. Other factors such as crystal-crystal adhesion forces are likely to additionally affect ϕ^* .

5. The addition of effective PPD polymers causes ϕ^* to increase which decreases the pour point temperature. Because ϕ^* weakly correlates with axial ratio (h/d), it is concluded that effective PPD polymers work, in part, by changing the axial ratio of the precipitated wax crystals.
6. In agreement with arguments based on PPD polymer-solvent affinity and its tendency to adsorb to a wax crystal, it is observed that pour point depression efficacy in systems containing 20 wt% wax is maximum when the PPD polymer solubility temperature is approximately 15 °C lower than the wax solubility temperature. Measurement of the PPD solubility temperature potentially offers a simple, rapid screening test for the identification of PPD candidates likely to be effective in particular wax/solvent systems.

Acknowledgements

We thank Lubrizol, Hazelwood, UK for supplying the PPD polymer samples and for provision of a PhD studentship for Noel A. Roberts.

Supporting Information Available:

- ESI Table 1. Structure and characterisation data for the PPD polymers.
- ESI Figure 1. Temperature hysteresis of the wax solubility boundary.
- ESI Figure 2. PPD polymer solubilities versus temperature.
- ESI Figure 3. Variation of pour point temperature with C24 wax concentration in toluene for different concentrations of LMn-MSA-C12 (upper plot) and LMn-MSA-C18-22 (lower plot).
- ESI Figure 4. Examples of wax crystal SEM images showing the arrowed dimensions of individual crystals used to construct the cumulative distribution plots for h and d.
- ESI Table 2. Results of repeated experiments to determine the reproducibility/repeatability of h and d values.
- ESI Figure 5. Cumulative distributions of h and d for different initial wax concentrations and for different temperature conditions.
- ESI Figure 6. Variation of polymer PPD efficacy (plotted as $(\phi^*_{1\text{wt}\%PPD} - \phi^*_{\text{noPPD}})$) versus the difference in polymer PPD and wax solubility temperatures using T_{heat} values for 50 and 100 wt% wax.

References

1. D.J. Abdallah and R.G. Weiss, *Langmuir*, 2000, **16**, 352-355.
2. R.F.G. Visintin, R. Lapasin, E. Vignati, P. D'Antona and T.P. Lockhart, *Langmuir*, 2005, **21**, 6240-6249.
3. E. Vignati, R. Piazza, R.F.G. Visintin, R. Lapasin, P. D'Antona and T.P. Lockhart, *J. Phys. Condens. Matter*, 2005, **17**, S3651-S3660.
4. K. Higaki, Y. Sasakura, T. Koyano, I. Hachiya and K. Sato, *J. Amer. Oil Chem. Soc.*, 2003, **80**, 263-270.
5. G.A. Holder and J. Winkler, *Nature*, 1965, **207**, 719-721.
6. G.A. Holder and D. Macauley, *Polym. Int.*, 1992, **28**, 47-53.
7. I.G. Davidson and G.G. Cameron, *Macromol.*, 1995, **28**, 5964-5966.
8. A.J. Hennessy, A. Neville and K.J. Roberts, *J. Crystal Growth*, 1999, **198/199**, 830-837.
9. J.W. Qian, J. Li, G.H. Zhou and G.R. Qi, *J. Appl. Polym. Sci.*, 2000, **78**, 836-841.
10. M. Del Carmen Garcia, L. Carbognani, M. Orea and A. Urbina, *J. Pet. Sci. Eng.*, 2000, **25**, 99-105.
11. J.S. Manka and K.L. Ziegler, *Soc. Pet. Eng. Paper 67326*, 2001.
12. J.W. Qian, G.H. Zhou, W.Y. Yang and Y.L. Xu, *J. Appl. Polym. Sci.*, 2002, **83**, 815-821.
13. H.S. Ashbaugh, A. Radulescu, R.K. Prud'homme, D. Schwahn, D. Richter and L.J. Fetters, *Macromol.* 2002, **35**, 7044-7053.
14. H.S. Ashbaugh, L.S. Fetters, D.H. Adamson and R.K. Prud'homme, *J. Rheol.*, 2002, **46**, 763-776.
15. K.S. Pedersen and H.P. Ronningsen, *Energy & Fuels*, 2003, **17**, 321-328.
16. X. Guo, B.A. Pethica, J.S. Huang, R.K. Prud'homme, D.H. Adamson and L.J. Fetters, *Energy & Fuels*, 2004, **18**, 930-937.
17. H.S. Ashbaugh, X. Guo, D. Schwahn, R.K. Prud'homme, D. Richter and L.J. Fetters, *Energy & Fuels*, 2005, **19**, 138-144.
18. E. Marie, Y. Chevalier, F. Eydoux, L. Germanaud and P. Flores, *J. Colloid Interface Sci.*, 2005, **290**, 406-418.
19. X. Guo, B.A. Pethica, J.S. Huang, D.H. Adamson and R.K. Prud'homme, *Energy & Fuels*, 2006, **20**, 250-256.
20. T. Yu, J. Wang and J. Jin, *Energy Sources Part A*, 2006, **28**, 757-762.
21. S.A. Mahmoud, T.T. Khidir and F.M. Ghuiba, *Pet. Sci. Technol.*, 2006, **24**, 1115-1124.
22. A. Radulescu, D. Schwahn, J. Stellbrink, E. Kentzinger, M. Heiderich and D. Richter, *Macromol.* 2006, **39**, 6142-6151.
23. A. Radelescu, L.J. Fetters and D. Richter, *Adv. Polym. Sci.*, 2008, **210**, 1-100.
24. H.P. Soni, Kiranbala and D.P. Barambe, *Energy & Fuels*, 2008, **22**, 3930-3938.
25. W.H. Chen, X.D. Zhang, Z.C. Zhao and C.Y. Yin, *Fluid Phase Equil.*, 2009, **280**, 9-15.
26. W. Chen, Z. Zhao and C. Yin, *Fuel*, 2010, **89**, 1127-1132.
27. S. Han, K. Zeng, H. Lin and P. Wang, *Chem. Technol Fuels Oils*, 2010, **46**, 309-318.
28. O.A.A. El-Shamy, T.T. Khid and M.M. Doheim, *J. Disp. Sci. Technol.*, 2011, **32**, 654-658.
29. S. Yi and J. Zhang, *Energy & Fuels*, 2011, **25**, 1686-1696.
30. S. Deshmukh and D. Barambe, *J. Disp. Sci. Technol.*, 2011, **32**, 2910297.
31. L. Li, X. Guo, D.H. Adamson, B.A. Pethica, J.S. Huang and R.K. Prud'homme, *Ind. Eng. Chem. Res.*, 2011, **50**, 316-321.
32. L. Li, J. Xu, J. Tinsley, D.H. Adamson, B.A. Pethica, J.S. Huang, R.K. Prud'homme and X. Guo, *Env. Energy Eng.*, 2012, **58**, 2254-2261.
33. H.R.J. Ansaroudi, M. Vafaie-Sefti, Sh. Masoudi, T.J. Behbahani and H. Jafari, *Pet. Sci. Technol.*, 2013, **31**, 643-651.
34. D.M. Duffy and P.M. Rodger, *Phys. Chem. Chem. Phys.*, 2002, **4**, 328-334.

35. D.M. Duffy, C. Moon and P.M. Rodger, *Molec. Phys.* 2004, **102**, 203-210.
36. J. Zhang, M. Zhang, J. Wan and W. Li, *J. Phys. Chem. B*, 2008, **112**, 36-43.
37. ASTM. Designation: D97-09 Standard test method for pour point of petroleum products. 2009.
38. I.Z. Schroder, *Z. Physik. Chem.*, 1893, **11**, 449-465.
39. H. Le Chatelier, *Compte. Rend.*, 1894, **118**, 638-641.
40. C.M.L. Atkinson and M.J. Richardson, *Trans. Faraday Soc.*, 1969, **65**, 1749-1763.
41. W.R. Turner, *Ind. Eng. Chem. Prod. Res. Develop.*, 1971, **10**, 238-260.
42. E.B. Sirota, H.E. King Jr., D.M. Singer and H.H. Shao, *J. Chem. Phys.*, 1993, **98**, 5809-5824.
43. S.P. Srivastava, J. Handoo, K.M. Agrawal and G.C. Joshi, *J. Phys. Chem. Solids*, 1993, **54**, 639-670.
44. E.B. Sirota and D.M. Singer, *J. Chem. Phys.*, 1994, **101**, 10873-10882.
45. S.R. Craig, G.P. Hastie, K.J. Roberts and J.N. Sherwood, *J. Mater. Chem.*, 1994, **4**, 977-981.
46. A. Hammami and A.K. Mehotra, *Fuel*, 1995, **74**, 96-101.
47. M. Dirand, M. Bouroukba, V. Chevallier, D. Petitjean, E. Behar and V. Ruffier-Meray, *J. Chem. Eng. Data*, 2002, **47**, 115-143.
48. H.E.L. Madsen and R. Boistelle, *J. Chem. Soc. Faraday Trans. 1*, 1976, **72**, 1078-1081.
49. S-S. Chang, J.R. maurey and W.J. Pummey, *J. Chem. Eng. Data*, 1983, **28**, 187-189.
50. M-C. Haulait-Pirson, G. Huys and E. Vanstraelen, *Ind. Eng. Chem. Res.*, 1987, **26**, 447-452.
51. U. Domanska and J. Rolinska, *Fluid Phase Equil.*, 1989, **45**, 25-38.
52. H.P. Ronningsen and B. Bjorndal, *Energy & Fuels*, 1991, **5**, 895-908.
53. A.B. Hansen, E. Larsen, W.B. Pedersen and A.B. Nielsen, *Energy & Fuels*, 1991, **6**, 914-923.
54. J.M. Letoffe, P. Claudy, M.V. Kok, M. Garcin and J.L. Volle, *Fuel*, 1995, **6**, 810-817.
55. J.A.P. Coutinho, S.I. Andersen, E. H. Stenby, *Fluid Phase Equil.*, 1995, **103**, 23-39.
56. C. Lira-Galeana, A. Firoozabadi and J.M. Prausnitz, *AIChE J.*, 1996, **42**, 239-248.
57. J. Pauly, C. Daupohin and J.L. Daridon, *Fluid Phase Equil.*, 1998, **149**, 191-207.
58. E. Provost, V. Chevallier, M. Bouroukba, D. Petitjean and M. Dirand, *J. Chem. Eng Data*, 1998, **43**, 745-749.
59. P.M. Ghogomu, E. Provost, M. Bouroukba, M. Dirand and M. Hoch, *J. Thermal Anal.*, 1998, **53**, 49-56.
60. S. Kato, D. Hoshino, H. Noritomi and K. Nagahama, *Fluid Phase Equil.*, 2004, **219**, 41-47.
61. J.A.P. Coutinho, C. Goncalves, I.M. Marrucho, J. Pauly and J-L. Daridon, *Fluid Phase Equil.*, 2005, **233**, 28-33.
62. J.A.P. Coutinho, F. Mirante and J. Pauly, *Fluid Phase Equil.*, 2006, **247**, 8-17.
63. J.A.P. Coutinho, B. Edmonds, T. Morwood, R. Szczepanski and X. Zhang, *Energy & Fuels*, 2006, **20**, 1081-1088.
64. B. Coto, C. Martos, J.J. Espada, M.D. Robustillo and J.L. Pena, *Fuel*, 2010, **89**, 1087-1094.
65. E. Ghanaei, F. Esmaeilzadeh and J. Fathikalajahi, *Fuel*, 2012, **99**, 235-244.
66. W. Wang, K. Wu, J. Duan, P. Wang and J. Gong, *Adv. Mech. Eng.*, 2013, article ID:829591, 1-8.
67. P.J. Lu, E. Zaccarelli, F. Ciulla, A.B. Schofield, F. Sciortino and D.A. Weitz, *Nature*, 2008, **453**, 499-504.
68. A. Toda, H. Miyaji, Y. Ogawa and K. Takamizawa, *J. Mater. Sci.*, 1991, **26**, 2793-2796.
69. X-Y. Liu and P. Bennema, *J. Cryst. Gr.*, 1994, **135**, 209-223.
70. X-Y. Liu and P. Bennema, *Phys. Rev. B*, 1994, **49**, 765-775.
71. X-Y. Liu and P. Bennema, *Phys. Rev. B*, 1996, **53**, 2314-2325.
72. B.D. Chen and J. Garside, *J. Cryst. Gr.*, 1996, **166**, 1094-1098.
73. P.J.C.M. van Hoof, R.F.P. Grimbergen, H. Meekes, W.J.P. van Enkevort and P. Bennema, *J. Cryst. Gr.*, 1998, **191**, 861-872.

74. P.J.C.M. van Hoof, W.J.P. van Enkevort, M. Schousten, P. Bennema and X.Y. Liu, *J. Cryst. Gr.*, 1998, **183**, 641-652.
75. M. Plomp, W.J.P. van Enkevort, P.J.C.M. van Hoof and C.J. van de Streek, *J. Cryst. Gr.*, 2003, **249**, 600-613.
76. M.K. Chaudhury, *Mater. Sci. Eng.*, 1996, **R16**, 97-159.
77. P.A. Forsyth Jr., S. Marcelja, D.J. Mitchell and B.W. Ninham, *J. Chem. Soc. Faraday Trans II*, 1977, **73**, 84-88.
78. D. Frenkel and R. Eppenga, *Phys. Rev. Lett.*, 1982, **49**, 1089-1092.
79. J.A.C. Veerman and D. Frenkel, *Phys. Rev. A.*, 1992, **45**, 5632-5648.
80. F.M. van der Kooij, K. Kassapidou and H.N.W. Lekkerkerker, *Nature*, 2000, **406**, 868-871.
81. A.J. Guenther and T. Kyu, *J. Polym. Sci. B*, 2000, **38**, 2366-2377.
82. A. Donev, S. Torquato, F.H. Stillinger and R. Connelly, *J. Appl. Phys.*, 2004, **95**, 989-999.
83. P. Jalali and M. Li, *Physica A*, 2007, **381**, 230-238.
84. A.J.W. ten Brinke, L. Bailey, H.N.W. Lekkerkerker and G.C. Maitland, *Soft Matter*, 2007, **3**, 1145-1162.
85. H.H. Wensink and H.N.W. Lekkerkerker, *Mol. Phys.*, 2009, **107**, 2111-2118.
86. M. Marechal, A. Cuetos, B. Martinez-Haya and M. Dijkstra, *J. Chem. Phys.*, 2011, **134**, 094501-1-12.
87. L. Wu, H.H. Wensink, G. Jackson and E.A. Muller, *Mol. Phys.* 2012, **110**, 1269-1288.
88. L. Wu, G. Jackson and E.A. Muller, *Int. J. Mol. Sci.*, 2013, **14**, 16414-16442.
89. E. Velasco and Y. Martinez-Raton, *Phys. Chem. Chem. Phys.*, 2014, **16**, 765-775.

Table 1. Phase transition temperatures and enthalpy changes for the three pure waxes used here. The data is taken from ref. 47.

Wax	T_{rot}/ °C	T_{liq}/ °C	ΔH_{rot}/ J mol⁻¹	ΔH_{liq}/ J mol⁻¹
Eicosane C20	-	36.4	-	69730
Tetracosane C24	47.6	50.5	31701	54396
Hexatriacontane C36	73.9	75.8	31071	87682

Table 2. Summary of wax critical volume fractions at the pour point (ϕ^*), wax crystal axial ratios (h/d) and solubility temperatures for 1 wt% polymer and 20 wt% wax solutions. Measurements of (h/d) for C20 wax were not possible as exposure to the SEM caused crystal melting (indicated as “n.d.” – “not determined” in the table).

Wax	Solvent	Polymer	$\phi^*/\text{vol}\%$	(h/d)	T_{heat} for 1 wt% polymer/ °C (in the absence of wax)	T_{heat} for 20 wt% wax/°C
C20	Heptane	None	5.5	n.d.	-	9.3
	Toluene	None	1.5	n.d.	-	10.7
C24	Heptane	None	7.4	0.0064	-	24.5
	Toluene	None	4.5	0.0054	-	24.0
C36	Heptane	None	2.9	0.0050	-	51.0
	Toluene	None	3.5	0.016	-	49.8
C20	Heptane	HMn-MS-C18-22	10.4	n.d.	25.0	9.3
		LMn-MS-C18-22	12.2	n.d.	26.0	9.3
		LMn-MSA-C18-22	8.5	n.d.	26.5	9.3
		LMn-MSA-C12	7.1	n.d.	< -10.0	9.3
	Toluene	HMn-MS-C18-22	8.8	n.d.	7.8	10.7
		LMn-MS-C18-22	7.5	n.d.	13.9	10.7
		LMn-MSA-C18-22	8.6	n.d.	16.4	10.7
		LMn-MSA-C12	1.7	n.d.	< -10.0	10.7
		HMn-MS-C18-22	12.3	0.011	25.0	24.5
		LMn-MS-C18-22	13.0	0.013	26.0	24.5
C24	Heptane	LMn-MSA-C18-22	10.6	0.019	26.5	24.5
		LMn-MSA-C12	5.1	0.0083	< -10.0	24.5
		HMn-MS-C18-22	14.0	0.043	7.8	24.0
		LMn-MS-C18-22	14.8	0.044	13.9	24.0
	Toluene	LMn-MSA-C18-22	13.3	0.016	16.4	24.0
		LMn-MSA-C12	3.8	0.0046	< -10.0	24.0
		HMn-MS-C18-22	7.7	0.030	25.0	51.0
		LMn-MS-C18-	13.3	0.026	26.0	51.0

		22				
		LMn-MSA-C18-22	7.6	0.022	26.5	51.0
		LMn-MSA-C12	3.0	0.0055	< -10.0	51.0
	Toluene	HMn-MS-C18-22	7.4	0.027	7.8	49.8
		LMn-MS-C18-22	8.6	0.013	13.9	49.8
		LMn-MSA-C18-22	7.5	0.011	16.4	49.8
		LMn-MSA-C12	3.4	0.012	Polymer solubility transition not visible	49.8

Figure 1. Variation of wax solubility with temperature for C20 (squares), C24 (triangles) and C36 (circles) in heptane (upper plot) and toluene (lower plot) as solvent. The curved dashed lines show the ideal solution solubility behaviour predicted using the parameters shown in Table 1.

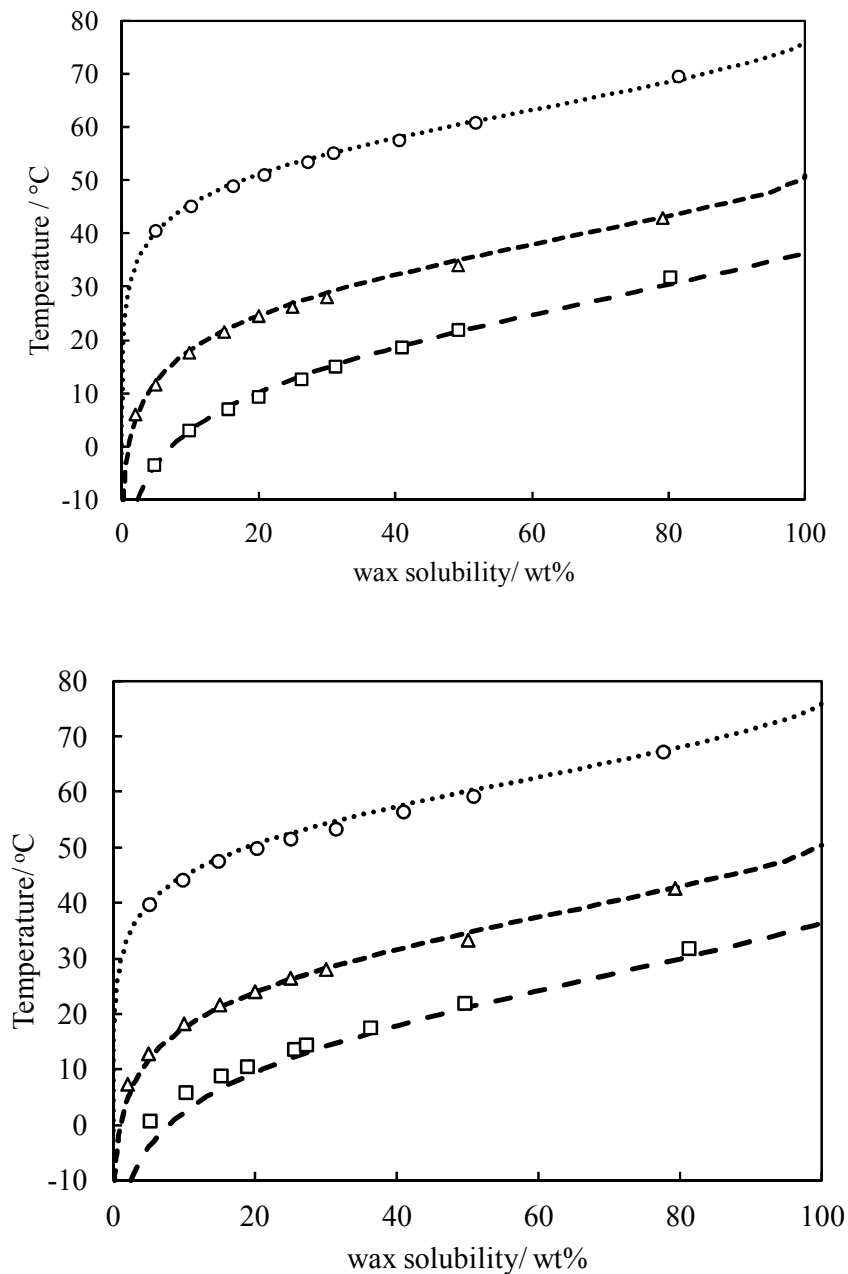


Figure 2. Pour point temperature versus wax concentration for C24 (filled triangles) and C36 (filled circles) in heptane as solvent with no added PPD polymer. The curved dashed lines show the ideal solution solubility behaviour predicted using the parameters shown in Table 1. The solid lines are calculated as described in the text using the values of critical volume fraction ϕ^* shown in Table 2.

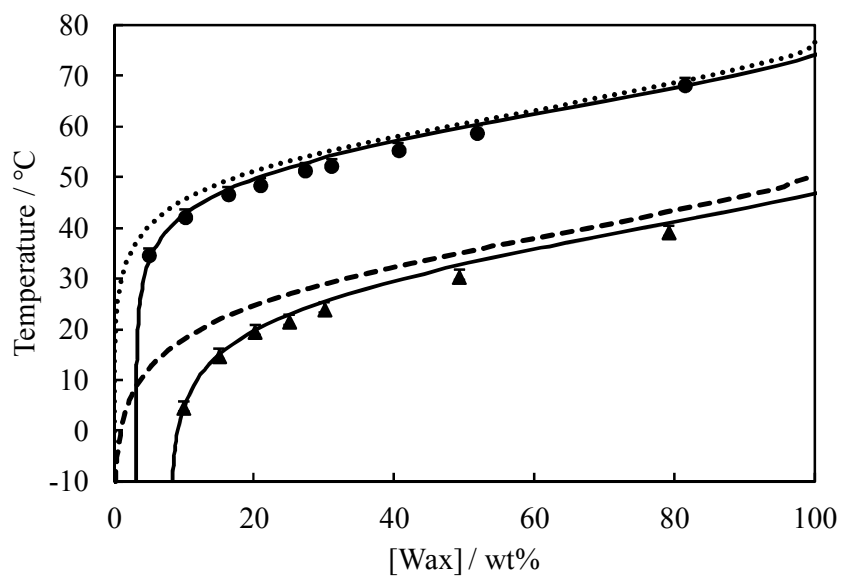
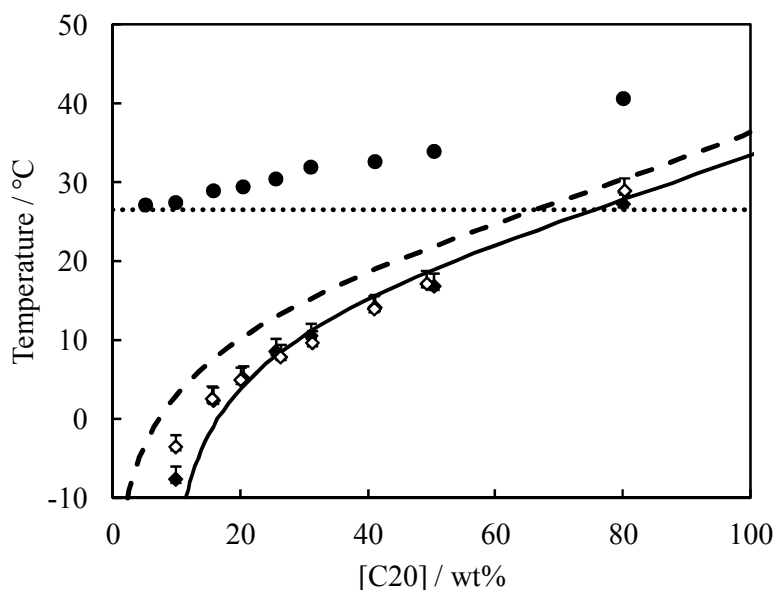


Figure 3. Variation of pour point temperature with wax concentration in the absence (unfilled diamonds) and presence (filled diamonds) of 1 wt% PPD polymer. The curved dashed lines show the ideal solution solubility behaviour for the wax predicted using the parameters shown in Table 1. The horizontal dotted line shows the solubility boundary of the 1 wt% PPD polymer in the absence of wax. The filled circles show the first solubility boundary temperatures observed on cooling solutions containing wax and 1 wt% PPD polymer as a function of the wax concentration. (For the upper plot, this data corresponds to the polymer solubility in the presence of wax whereas in the lower two plots, the data corresponds to the wax solubility in the presence of polymer.) The curved solid lines are the calculated best-fits to the pour point temperatures in the presence of PPD polymer using the values of critical volume fraction ϕ^* shown in Table 2.

Upper plot: C20 wax in heptane with and without 1 wt% LMn-MSA-C18-22
 Middle plot: C36 wax in heptane with and without 1 wt% LMn-MS-C18-22
 Lower plot: C20 wax in heptane with and without 1 wt% LMn-MSA-C12 (The polymer solubility boundary is less than -10 °C and is not shown.)



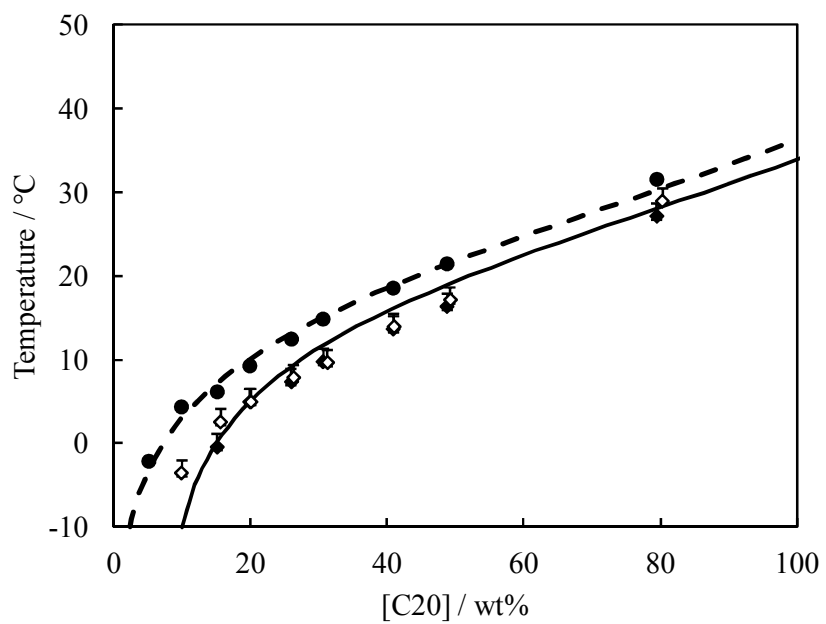
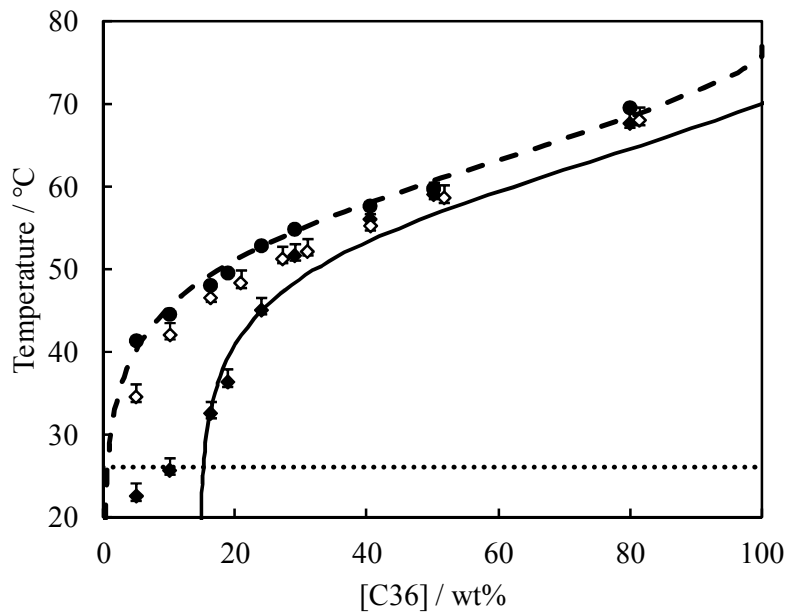
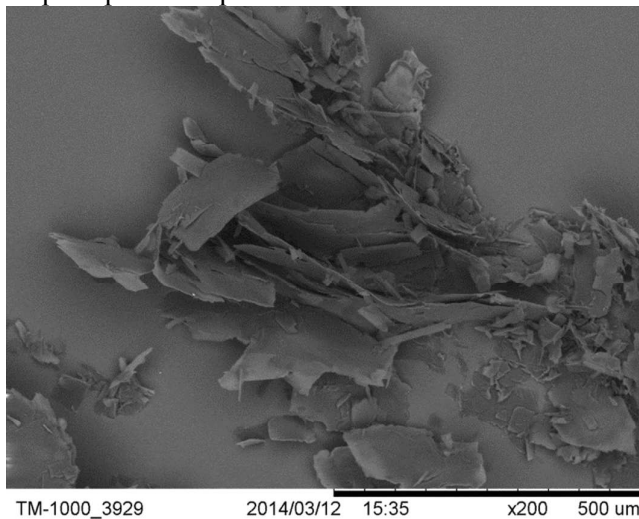
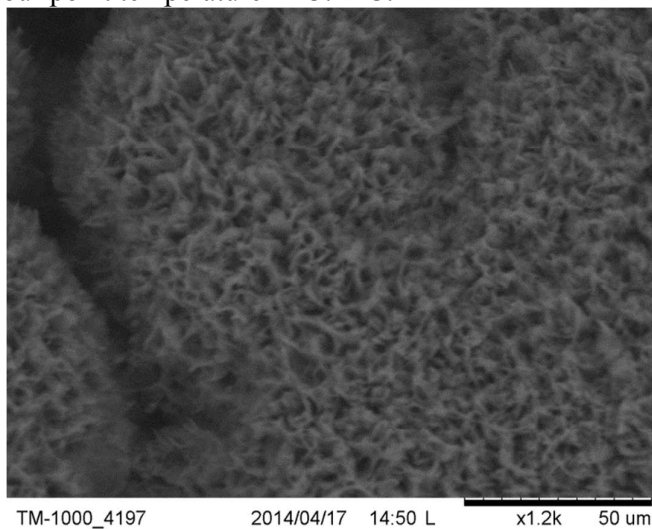


Figure 4. Examples of SEM images of extracted wax crystals.

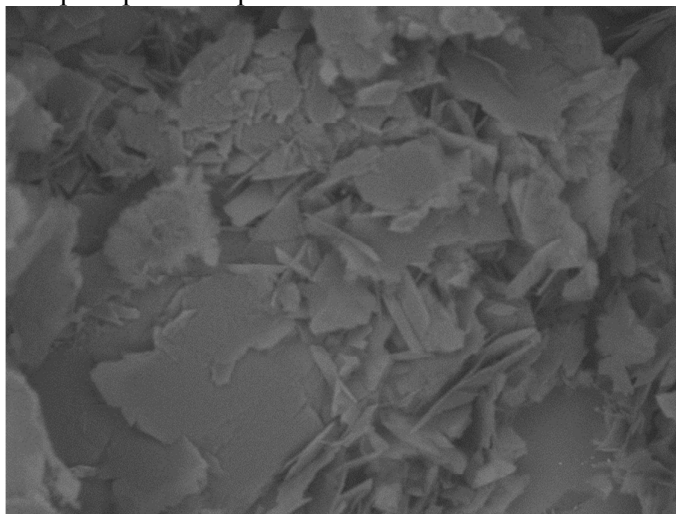
- (i) C24 crystals extracted from a 20 wt% solution in toluene in the absence of PPD polymer. Crystal extraction temperature = 21.5 °C, solubility boundary temperature = 24.1 °C and pour point temperature = 22.0 °C.



- (ii) C24 crystals extracted from a 20 wt% solution in toluene with 1 wt% LMn-MS-C18-22. Crystal extraction temperature = 13.6 °C, solubility boundary temperature = 24.7 °C and pour point temperature = 13.1 °C.

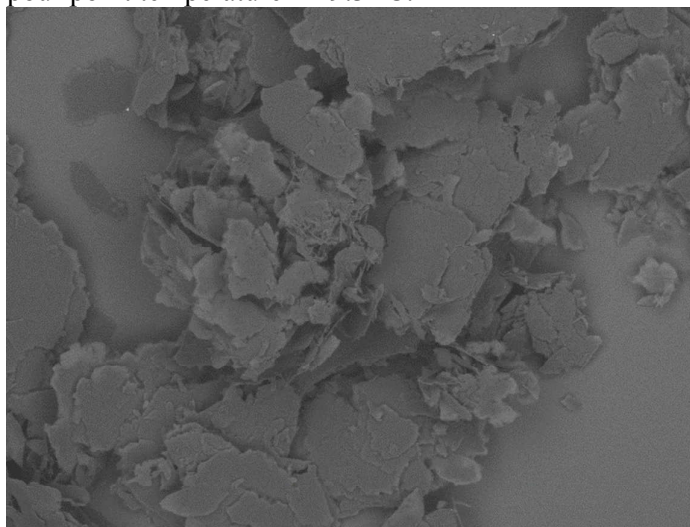


- (iii) C36 crystals extracted from a 20 wt% solution in heptane in the absence of PPD polymer. Crystal extraction temperature = 48.0 °C, solubility boundary temperature = 50.7 °C and pour point temperature = 49.8 °C.



TM-1000_4149 2014/04/17 11:28 L x200 500 um

- (iv) C36 crystals extracted from a 20 wt% solution in heptane with 1 wt% LMn-MSA-C12. Crystal extraction temperature = 47.3 °C, solubility boundary temperature = 49.7 °C and pour point temperature = 49.3 °C.



TM-1000_4043 2014/06/03 12:06 L x100 1 mm

Figure 5. Upper plot: cumulative distributions of h (triangles) and d (circles) for 20 wt% C24 in toluene with (filled points) and without (unfilled points) 1 wt% LMn-MS-C18-22 (derived from the images in Figure 4(i) and (ii)). Lower plot: cumulative distributions of h (triangles) and d (circles) for 20 wt% C36 in heptane with (filled points) and without (unfilled points) 1 wt% LMn-MSA-C12 (derived from the images in Figure 4(iii) and (iv))

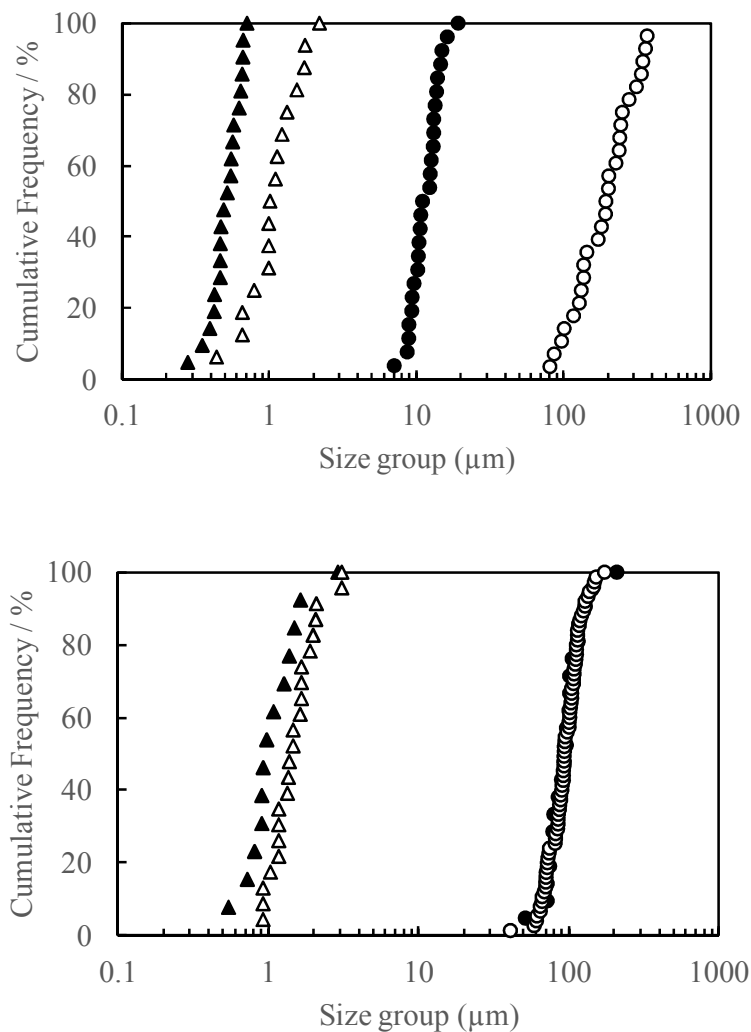


Figure 6. Variation of measured critical volume fraction of crystals ϕ^* (derived from pour point temperature measurements) versus average crystal axial ratio h/d from SEM for all systems. The dashed lines correspond to $\phi^* = 2.5(h/d)$ and $\phi^* = 11(h/d)$.

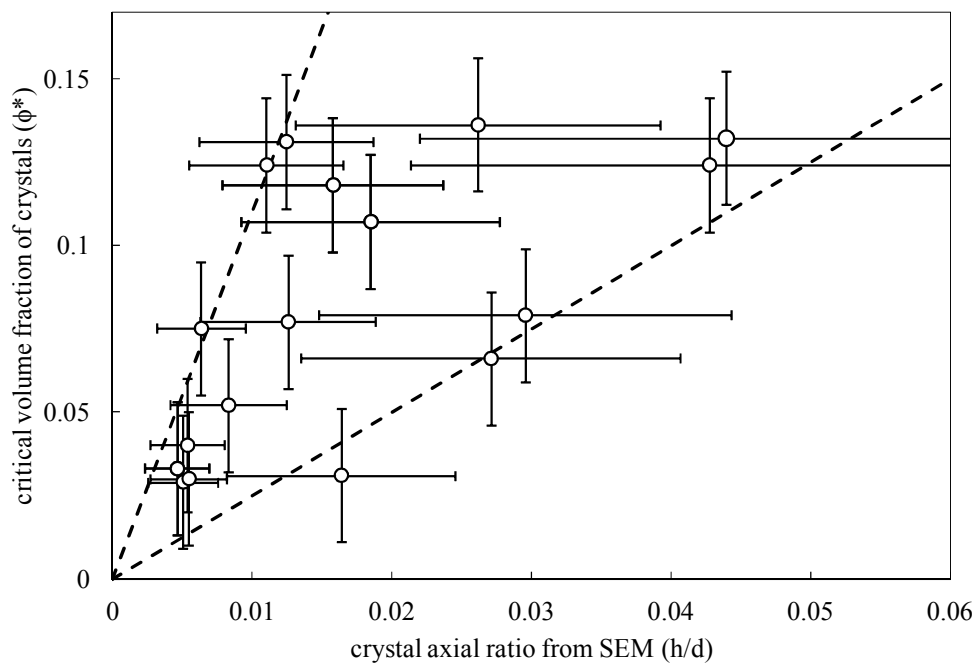


Figure 7. Variation of polymer PPD efficacy (plotted as $(\phi^*_{1\text{wt}\% \text{PPD}} - \phi^*_{\text{noPPD}})$) versus the difference in polymer PPD and wax solubility temperatures ($T_{\text{heat}1\text{wt}\% \text{PPD}} - T_{\text{heat}20\text{wt}\% \text{wax}}$) for all wax/solvent/PPD systems. The unfilled symbols refer to systems containing LMn-MSA-C12 for which the solubility temperature in both solvents was determined only as being less than $-10\text{ }^\circ\text{C}$; for these data points the true position on the relative temperature scale is somewhere *below* the position plotted (using $-10\text{ }^\circ\text{C}$ as the PPD solubility temperature). The horizontal solid line marks zero pour point depression and the curved dashed line is a guide for the eye.

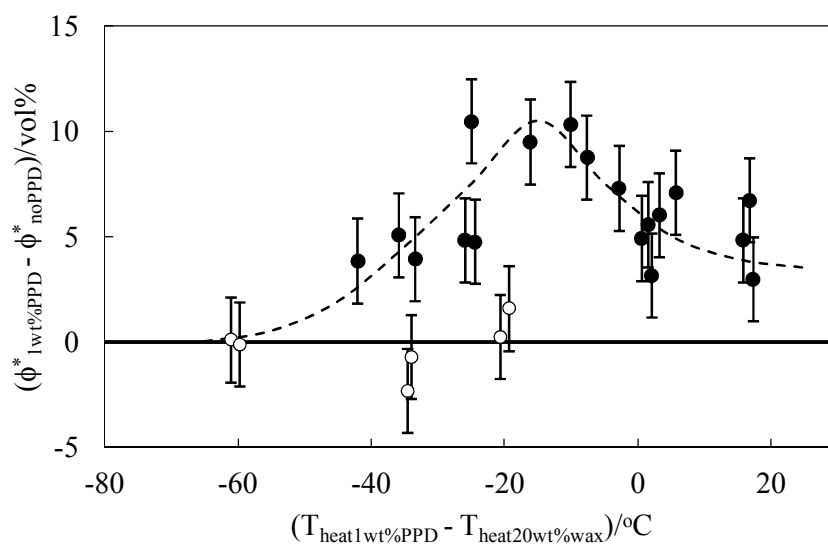


Table of Contents Graphic

We show how polymer additives reduce the pour point temperature of wax solutions in hydrocarbon solvents.

